

Critical role of substrate in the high temperature superconductivity of single layer FeSe on Nb:BaTiO₃

R. Peng,^{1,*} H. C. Xu,^{1,*} S. Y. Tan,¹ M. Xia,¹ X. P. Shen,¹ Z. C. Huang,¹
C. H. P. Wen,¹ Q. Song,¹ T. Zhang,¹ B. P. Xie,¹ and D. L. Feng^{1,†}

¹State Key Laboratory of Surface Physics, Department of Physics,
and Advanced Materials Laboratory, Fudan University, Shanghai 200433, People's Republic of China
(Dated: January 22, 2021)

In the quest for high temperature superconductors, the interface between a metal and a dielectric was proposed to possibly achieve very high superconducting transition temperature (T_c) through interface-assisted pairing^{1,2}. Recently, in single layer FeSe (SLF) films grown on SrTiO₃ substrates, signs for T_c up to 65 K have been reported^{3,4}. However, besides doping electrons and imposing strain, whether and how the substrate facilitates the superconductivity are still unclear. Here we report the growth of various SLF films on thick BaTiO₃ films atop KTaO₃ substrates, with signs for T_c up to 75 K, close to the liquid nitrogen boiling temperature. SLF of similar doping and lattice is found to exhibit high T_c only if it is on the substrate, and its band structure strongly depends on the substrate. Our results highlight the profound role of substrate on the high- T_c in SLF, and provide new clues for understanding its mechanism.

The record T_c has long been 56 K for the bulk iron-based high temperature superconductors (Fe-HTS's). Recently, in SLF films grown on Nb doped SrTiO₃ (NSTO) substrate (hereafter referred as FeSe^S) by molecular beam epitaxy (MBE), both scanning tunneling spectroscopy and angle-resolved photoemission spectroscopy (ARPES) experiments have observed large superconducting gap^{5,6}, which closes at ~65 K (ref. 3,4). On the other hand, *ex situ* transport measurements of SLF films capped with FeTe and silicon show an onset T_c of about 40 K, with signs for a possible Berezinskii-Kosterlitz-Thouless (BKT) transition⁷. Although whether this is the true T_c remains to be checked by *in-situ* transport measurements, it is likely that the phase fluctuation in this two dimensional system is strong, so that the ARPES gap-closing temperature, T_g , only measures the Cooper pair formation temperature, instead of T_c . Nevertheless, it implies that a T_c equivalent to T_g can be achieved if the fluctuations in such a two dimensional system could be suppressed.

Based on the existing experiments, the NSTO substrate affects SLF in the following ways. 1. The oxygen vacancies in the substrate induces extra electrons that are transferred to the interfacial FeSe layer^{4,8}, which suppresses the antiferromagnetism in SLF and allows for a high T_g (ref. 4). 2. The in-plane lattice constant (a) of NSTO is 3.905 Å, thus it imposes a large tensile strain on SLF, noting $a=3.765$ Å for bulk FeSe. It was shown that the tensile strain would enhance the antiferromagnetic interactions in FeSe (ref. 9). However, for SLF films with extremely expanded a of ~3.99 Å in epitaxially grown FeSe/NSTO/KTaO₃ heterostructures (hereafter referred as FeSe^{SX}), the T_g increases just moderately to about

70 K (ref. 10). 3. It was reported recently that electrons in FeSe might interact with an ~80 meV optical phonon in the substrate¹¹. So far, it is still unclear whether and how the substrate plays a more direct role in mediating the superconducting pairing in SLF.

To study the role of substrate in SLF superconductivity, different substrates should be examined. BaTiO₃ (BTO) can be made with the same TiO₂ termination as STO. However, due to the spontaneous polarization of BTO, atomically flat surface is hard to obtain with bulk BTO. To overcome this, since BTO lattice ($a=3.992$ Å) is merely 0.075 % larger than that of KTaO₃ (KTO), we first grew >40 u.c. of Nb-doped BTO (NBTO, to provide a conducting substrate) on the (001) surface of a KTO crystal by ozone assisted MBE, then grew SLF on the NBTO film (Fig. 1a) as described in the Methods section. This heterostructure, hereafter referred as FeSe^B, is then transferred to the analysis chamber under ultra high vacuum for the *in-situ* measurements of low energy electron diffraction (LEED) and ARPES.

The as-grown well-oxidized NBTO film exhibits a nice surface with the symmetry of the substrate, as shown by its LEED pattern in Fig. 1a. However, after heat treated at 950°C under the selenium flux, the NBTO film exhibits a 3×3 reconstruction. This has a direct impact on the SLF grown on it. The left part of Fig. 1b shows the photoemission intensity map at the Fermi energy (E_F) for FeSe^B, where three sets of Fermi surfaces are observed. One set (unrotated) is made of elliptical Fermi surface sheets, similar to that observed in FeSe^{SX} (ref. 10). The other two sets are made of more circular sheets, similar to the Fermi surface topology of FeSe^S film. Although these Fermi surface sheets appear to cross each other, their band structures do not exhibit any hybridization. This indicates that they are likely originated from three types of spatially separated domains. Moreover, the superstructure in the substrate does not cause any observable folding, indicating that the crystal potential of the substrate affects the FeSe rather weakly¹². The in-plane lattice constant a of each domain could be derived from the inverted Brillouin zone size determined by high symmetry points of photoemission map⁴. We found that one domain preserves the lattice of the KTO substrate ($a \sim 3.99$ Å), and the other two domains rotated about $\pm 18.5^\circ$ with $a \sim 3.78$ Å. Consistently, the LEED pattern of FeSe^B in Fig. 1b can be decomposed into three sets of spots. Besides the main spots that reflect the unrotated lattice of the substrate (highlighted by the blue square), there are spots corresponding to two $\pm 18.5^\circ$ rotated lattices (highlighted by the two yellow squares). As shown in Fig. 1e, these three domains of FeSe match the reconstructed substrate. Particularly, every

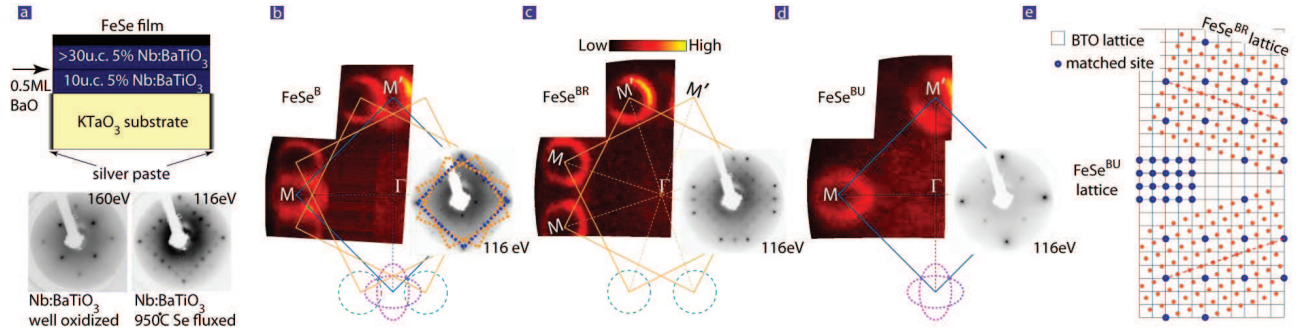


FIG. 1: The structure and Fermi surface of FeSe/Nb:BTO/KTO film. **a**, The schematic cross-section of the FeSe/Nb:BTO/KTO film. The LEED (low energy electron diffraction) patterns for the Nb:BTO/KTO film before and after the heat treatment under Se flux are shown on the bottom. To prepare for FeSe^{BU} growth, an extra 0.5 ML of BaO is inserted to eliminate the 3×3 superstructure as indicated. **b**, Left: the Fermi surface of a film named FeSe^B as represented by the photoemission intensity map at the Fermi energy. The intensity was integrated over a window of (E_F , E_F-20 meV). Right: its LEED pattern. Besides the main spots that reflect the unrelaxed lattice of the substrate (indicated by the blue square), there are spots corresponding to two $\pm 18.5^\circ$ rotated lattices (indicated by the yellow squares). Correspondingly, there are three sets of Fermi surfaces, whose respective Brillouin zone are derived based on the high symmetry points. **c**, Left: the Fermi surface of a film named FeSe^{BR} resulting from post-annealing FeSe^B, where only two sets of Fermi surfaces are observed, corresponding to the two $\pm 18.5^\circ$ rotated lattices. Right: its LEED pattern, where the main spots are weakened, and the spots for the rotated lattice are enhanced. **d**, Left: The Fermi surface of a film named FeSe^{BU}, where only the elliptical Fermi surface sheets are observed. Right: its LEED pattern. No superstructure spots are observed, and the lattice is unrelaxed. **e**, Sketches for the lattices of various FeSe/Nb:BTO/KTO films.

10 periods of the rotated FeSe lattice match the diagonal of a 3×9 rectangle of the NBTO lattice (the dashed line in Fig. 1e).

After post-annealing for over 15 hours (details are shown in the Supplementary Information), the $\pm 18.5^\circ$ domains with the relaxed lattice could be further enhanced (such a film is referred as FeSe^{BR} hereafter). As shown in Fig. 1c, the spots correspond to the rotated lattices become stronger, while those correspond to the unrelaxed lattice is weakened. As expected, the elliptical Fermi surfaces sheets is negligibly weak. Intriguingly, we found that if some extra BaO is inserted during the growth of NBTO film, as shown in Fig. 1a, the resulting FeSe film only contains single unrelaxed domain, as illustrated by its LEED pattern in Fig. 1d. Such an unrelaxed film is referred as FeSe^{BU} hereafter. Consistently, the Fermi surface topology only contains orthogonal ellipses. Based on the calculated Luttinger volume, there are 0.12 e^- excessive electrons per Fe for all these films, similar to those SLF on NSTO as well.

Fig. 2 presents the band dispersions for various SLF films grown on NBTO or NSTO. Fig. 2a,b gives the dispersions across Γ (0,0). The generic features for all films include a parabolic band, and a relative flat band at higher binding energy. For films grown on NBTO, the larger a correspond to a larger band mass of the parabolic band and smaller separations between the two bands (Fig. 2b(i),(ii)), indicating stronger correlation effects with expanded lattice. The same holds true for the two films grown on NSTO (Fig. 2b(iii),(iv)). Intriguingly, even though both the NBTO/KTO and NSTO/KTO were terminated with the same TiO₂ layers that have the similar amount of oxygen vacancies and same lattice constant of 3.989 Å, there are clear differences in the band dispersions for FeSe^{SX} and FeSe^{BU} (Fig. 2b(i),(iii)). The bands are flatter for SLF on NSTO than for SLF on NBTO. As summarized in Fig. 2f,g, the two characteristic quantities (band mass and band separation) fall on two separate curves as a function of a ,

which clearly indicates the substrates have a nontrivial effects on the correlation and electronic structure in the FeSe film on them. The substrates affect the bands around M (π , 0) as well (Fig. 2c,d). For the large $a=3.989$ Å, two electron bands are resolved for FeSe^{BU} and FeSe^{SX} but with different separations (Fig. 2d(i),(iii))¹⁰, while for FeSe^{BR} and FeSe^S, the two bands cannot be resolved⁴. However, the bandwidths of the electron bands are similar in all these films.

The superconducting properties of the FeSe films grown on the NBTO films are examined in Fig. 3. Fig. 3a shows the symmetrized energy distribution curves (EDC's) at low temperatures along a cut across the Fermi surface of the unrelaxed FeSe domains of FeSe^B. The dispersion exhibits a characteristic bending back behavior after passing the Fermi momentum. This is a hallmark of Bogliubov quasiparticle dispersion, and indicates that the gap is due to Cooper pair formation. The symmetrized EDC's at the normal state Fermi momenta could be used to identify the gap by the spectral weight suppression at E_F , which is minimally affected by the temperature broadening effects¹³. Fig. 3b presents the temperature dependence of the symmetrized EDC's at the Fermi momentum for the unrelaxed domains in FeSe^B, and the gap decreases with increasing temperature and eventually closes above 73 K. Fig. 3c-d shows the gap behavior of FeSe^{BR}, which closes above 68 K. The data for FeSe^{BU} shows rather weak coherence peaks, but with possible signs for T_g above 77 K (see Supplementary Information).

The temperature dependence of the gap is shown in Fig. 3e, which could be well fitted by the Bardeen-Cooper-Schrieffer (BCS) gap vs. temperature formula. This, together with the Bogliubov quasiparticle behavior of the dispersion, suggest that it relates to the Cooper pair formation, although *in-situ* transport is needed to check if $T_c = T_g$. The fitted T_g is 75 ± 2 K, and 70 ± 2 K for FeSe^B and FeSe^{BR}, respec-

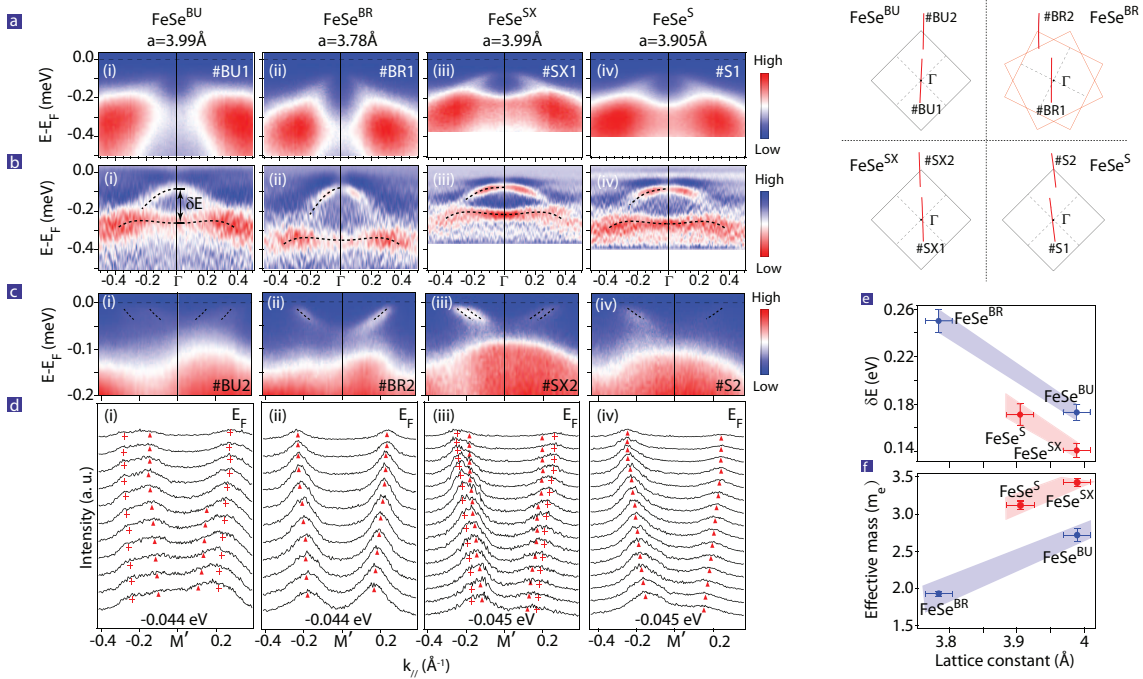


FIG. 2: **The band structure of various FeSe films.** **a,b**, The photoemission intensity **(a(i)-(iv))** and the corresponding second derivative with respect to energy to highlight the dispersions **(b(i)-(iv))** across the Γ for FeSe^{BU} , FeSe^{BR} , FeSe^{SX} , and FeSe^{S} , respectively. **c,d**, The photoemission intensity across M **(c(i)-(iv))**, and the corresponding momentum distribution curves (MDC's) **(d(i)-(iv))** for these films. **e** The separation between bands at Γ as defined in **b(i)** as a function of a . **f**, effective mass of the parabolic band at Γ as a function of a . The top-right inset illustrates the momentum locations for data in **a-d**. We note that the slight rotation of the cuts does not affect the quantitative conclusions here (see Supplementary Information). The #BU1 and #BR1 data were taken at 45 K, while others were taken at 30 K.

tively. The former sets a new record T_g for Fe-HTS's. Fig. 3f summarize the maximal gap versus T_g for FeSe films and $\text{K}_x\text{Fe}_{2-y}\text{Se}_2$. One can find a general linear trend between T_g and the gap amplitude, reflecting their superconducting nature. However, we note that the a 's of the FeSe^{BR} and FeSe^{BU} domains differ by 5.5%. When the lattice is expanded by such a large amount, the antiferromagnetic superexchange interactions across the Fe-Se-Fe would enhance significantly⁹. In the context of the antiferromagnetic-interaction/spin fluctuation mediated superconductivity, which is arguably the current dominating picture for bulk Fe-HTS's¹⁵, such a 5 K T_g difference is surprisingly small. In addition, there is no simple relation between the effective mass and T_g , while the increased correlation strength usually should help to enhance the superconductivity in such a high doping regime.

The a of FeSe^{BR} is close to that of bulk FeSe. It has been shown both by experiments and calculations that the undoped bulk FeSe has similar electronic structure as the iron pnictides with both electron and hole Fermi pockets^{4,16}. For iron pnictides, heavy electron doping would fill up the hole pockets, bring the system to the overdoped regime, and kill the superconductivity^{17,18}. To check if this is the case for FeSe, we have grown 35 u.c. thick cobalt-doped FeSe film on NSTO to introduce electron carriers (named $\text{FeCoSe}^{\text{SR}}$), and a is relaxed to about 3.78 Å in this film. As shown in Fig. 4a,b, the hole pockets of the α and β bands sink below the Fermi energy, and the electron Fermi surface is fairly large as shown

in Fig. 4c-e. About 8% electrons could be doped, which is limited by the solubility of cobalt. Fig. 4f,g shows no signs of a superconducting gap. The T_g , if any, is below the lowest temperature of 30 K that could be reached at the film. That is, for a SLF film with similar a and doping, it has a high T_g of $\sim 70\text{K}$ on NBTO, while its T_g is very low if such films are staked together in $\text{FeCoSe}^{\text{SR}}$. Had the superconductivity been originated only from the FeSe layer, one would expect the opposite: a higher T_g in $\text{FeCoSe}^{\text{SR}}$ due to suppressed fluctuations.

Our findings thus strongly suggest that interfacial effects could participate or even dominate the superconductivity in FeSe/NSTO or FeSe/NBTO. For example, one could speculate some intriguing and nonexclusive possibilities. For example, the polarizability of the ions in substrates induces interfacial electron-phonon interactions¹². The interactions between electrons and a substrate-originated phonon have been reported in FeSe^{S} (ref. 11). The high phonon frequency and strong electron phonon interactions in NSTO or NBTO may mediate superconductivity with high T_c as in BCS theory. It may also help enhance the antiferromagnetic-interaction mediated pairing as proposed in ref. 19 and 11. Moreover, Little¹ and Ginzburg² proposed almost half a century ago that the electronic polarizability of the substrate could introduce attractive force between electrons. This is unlikely here, since we did not find any noticeable dependence of the electronic structure and superconducting properties on the Nb concentration (*i.e.* conductivity and carrier density in the substrate).

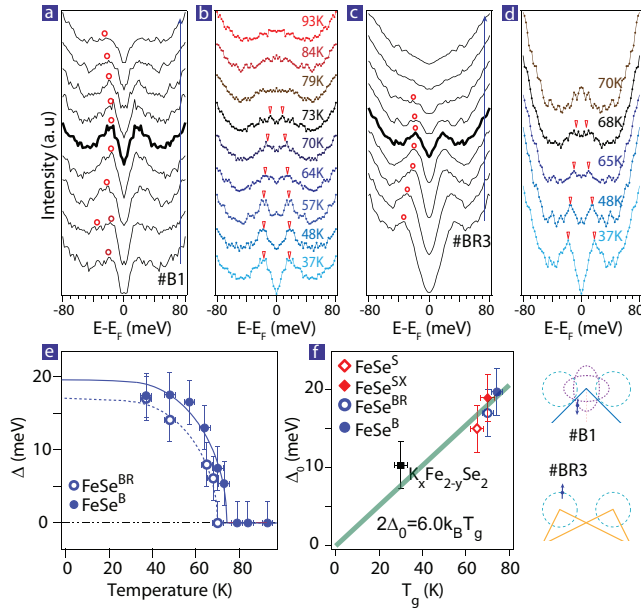


FIG. 3: Temperature dependence of the superconducting gap for FeSe films. **a**, The symmetrized energy distribution curves (EDC's) for FeSe^B along cut #B1 as indicated in the inset. The circles mark the dispersion. The thick EDC curve is at the normal state Fermi momentum (k_F). **b** Temperature dependence of the symmetrized EDC at the marked k_F for FeSe^B . The coherent peak positions are marked by triangles. **c,d**, similar as **a,b**, but for FeSe^{BR} film. **e**, The superconducting gap determined as a function of temperature from data in **b** and **d**. The solid lines are the fit for the gap-temperature dependence based on BCS theory. **f**, The maximal low temperature gap versus T_g plot, including the values for $\text{K}_x\text{Fe}_{2-y}\text{Se}_2$ bulk (ref. 14), FeSe^S (ref. 4) and FeSe^{SX} (ref. 10). Note for FeSe^{SX} and FeSe^B , the maximal values of the anisotropic gap distributions are used (see Supplementary Information).

Nevertheless, it would help to screen the Coulomb interactions at various ranges²⁰, thus facilitate pairing²¹. In fact, the observed substrate-dependence of correlations in FeSe may be resulting from the different screening of the interactions by NSTO and NBTO.

To summarize, we have successfully fabricated FeSe films on NBTO films, and enhance the gap-closing or Cooper-pair formation temperature up to 75 K. This establishes interface engineering as an effective path for enhancing T_c in SLF, and pave its way towards more cost-effective applications. More importantly, our data suggest that the substrate has a profound impact on the electronic structure in single layer FeSe/NSTO and FeSe/NBTO films, and their high temperature superconductivity probably results from an extraordinary interfacial mechanism. These results enrich the current understanding of interfacial superconductivity and high temperature superconductivity in general.

Methods:

Thin film growth

Over 40 unit cells of highly conductive 5% Nb doped BTO films were grown layer-by-layer on KTaO_3 (KTO) substrate with ozone-assisted molecular beam epitaxy (MBE). Dur-

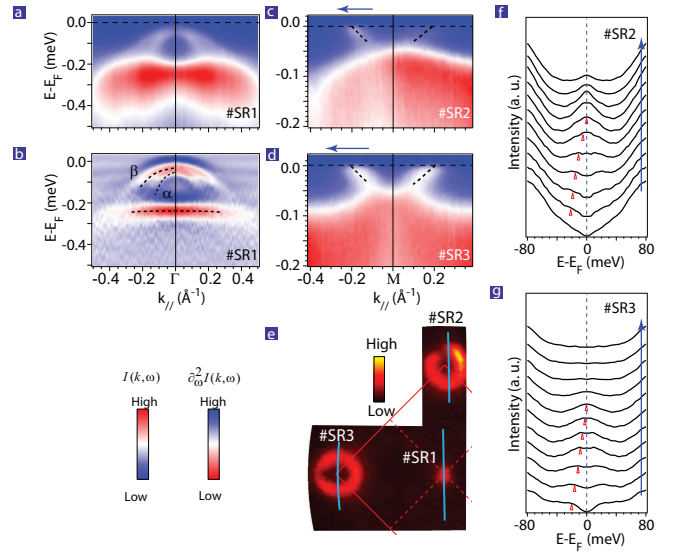


FIG. 4: Electronic structure of FeCoSe^{SR} . FeCoSe^{SR} is a Co doped thick FeSe film with relaxed lattice, $a=3.78 \text{ \AA}$. **a,b**, The photoemission intensity (**a**) and the corresponding second derivative with respect to energy to highlight the dispersions (**b**) along cut #SR1. **c,d**, The photoemission intensity along cut #SR2 and cut #SR3, respectively. **e**, Fermi surface map of FeCoSe^{SR} , where the momentum cuts for data in other panels are marked. **f,g**, The symmetrized EDC's along a portion of cut #SR2 (**f**) and cut #SR3 (**g**), as indicated by the blue arrows in **c** and **d**, respectively. The dispersions are marked by the red triangles. The data were taken at 30 K.

ing the growth of Nb:BTO, the reflection high-energy electron diffraction (RHEED) pattern retained its two dimensional character. With the shutter-controlled growth mode, the film is terminated with TiO_2 layer after the growth of each unit cell except for FeSe^{BU} (ref. 22). The Nb:BTO films were then transferred under an ultra-high vacuum to another MBE chamber, where heat treatment were performed, and then FeSe thin films were deposited following the procedure used in ref. 4. In this way, a FeSe/Nb:BTO/KTO heterostructure is fabricated.

ARPES measurement

ARPES data were taken *in situ* under ultra-high vacuum of $1.5 \times 10^{-11} \text{ mbar}$, with a SPECS UVLS discharge lamp (21.2eV He- α light) and a Scienta R4000 electron analyzer. The energy resolution is 8 meV and the angular resolution is 0.3° . Data were taken at 30 K if not specified otherwise. To eliminate the photoemission charging effect due to insulating KTO, silver paste was attached on the substrate edge before growth.

Acknowledgement: This work is supported in part by the National Science Foundation of China under the grant Nos. 91021001 and 91221303, and National Basic Research Program of China (973 Program) under the grant No. 2012CB921402.

Author contributions: R.P., H.C.X., S.Y.T., M.X., Q.S. and Z.C.Huang grew the films, R.P., H.C.X., S.Y.T., B.P.X., X.P.S., Z.C.Huang and C.H.P.Wen performed ARPES measurements. R. P., H.C.X., S.Y.T. and D.L.F. analyzed the ARPES data. D.L.F. and R.P. wrote the paper. D.L.F., B.P.X.,

and T.Z. are responsible for the infrastructure, project direction and planning.

Additional Information: The authors declare no compet-

ing financial interests. Correspondence and requests for materials should be addressed to D.L.F. (dlfeng@fudan.edu.cn).

-
- * These authors contributed equally to this work.
 † Electronic address: dlfeng@fudan.edu.cn
- ¹ Little, W. A. Possibility of synthesizing an organic superconductor. *Phys. Rev.* **134**, A1416-A1424 (1964).
 - ² Ginzburg, V. L. On surface superconductivity. *Physics Letters* **13**, 101-102 (1964).
 - ³ He, S. L. et al. Phase diagram and high temperature superconductivity at 65K in tuning carrier concentration of single-layer FeSe films. *Nature Mater.* **12**, 605-610 (2013).
 - ⁴ Tan, S. Y. et al. Interface-induced superconductivity and strain-dependent spin density wave in FeSe/SrTiO₃ thin films. *Nature Mater.* **12**, 634-640 (2013).
 - ⁵ Wang, Q. Y. et al. Interface induced high temperature superconductivity in single unit-cell FeSe films on SrTiO₃. *Chin. Phys. Lett.* **29**, 037402 (2012).
 - ⁶ Liu, D.F. et al. Electronic origin of high-temperature superconductivity in single-layer FeSe superconductor. *Nat. Commun.* **3**, 931 (2012).
 - ⁷ Zhang, W. et al. Direct observation of high temperature superconductivity in one-unit-cell FeSe films, *Chin. Phys. Lett.* **31**, 017401 (2014).
 - ⁸ Bang, J. , et al. Atomic and electronic structures of single-layer FeSe on SrTiO₃(001): The role of oxygen deficiency. *Phys. Rev. B* **87**, 220503 (2013).
 - ⁹ Cao, H. Y. , Tan, S. Y., Xiang, H. J., Feng, D. L. and Gong, X. G. The interfacial effects on the spin density wave in FeSe/SrTiO₃ thin film. Preprint at <http://arxiv.org/abs/1310.4024> (2013).
 - ¹⁰ Peng, R. et al. Enhanced superconductivity and evidence for novel pairing in single-layer FeSe on SrTiO₃ thin film under large tensile strain. Preprint at <http://arxiv.org/abs/1310.3060> (2013).
 - ¹¹ Lee J. J., et al. Evidence for pairing enhancement in single unit cell FeSe on SrTiO₃ due to cross-interfacial electron-phonon coupling. Preprint at <http://arxiv.org/abs/1312.2633> (2013).
 - ¹² Ou, H. et al. Novel electronic structure induced by a highly strained oxide interface with incommensurate crystal fields. *Phys. Rev. Lett.* **102**, 026806 (2009).
 - ¹³ Norman, M. R., Randeria, M., Ding, H. & Campuzano, J. C. Phenomenology of the low-energy spectral function in high-Tc superconductors. *Phys. Rev. B* **57**, R11093-R11096 (1998).
 - ¹⁴ Zhang Y. et al. Nodeless superconducting gap in A_xFe₂Se₂ (A=K, Cs) revealed by angle-resolved photoemission spectroscopy. *Nature Mater.* **10**, 273-277 (2011).
 - ¹⁵ Hu, J. & Ding, H. Local antiferromagnetic exchange and collaborative Fermi surface as key ingredients of high temperature superconductors. *Scientific Reports* **2**, 381 (2012).
 - ¹⁶ Ma, F. et al. First-principles calculations of the electronic structure of tetragonal α -FeTe and α -FeSe crystals: Evidence for a bicollinear AFM order. *Phys. Rev. Lett.* **102**, 177003 (2009).
 - ¹⁷ Liu, C. et al. Importance of the Fermi-surface topology to the superconducting state of the electron-doped pnictide Ba(Fe_{1-x}Co_x)₂As₂. *Phys. Rev. B* **84**, 020509 (2011).
 - ¹⁸ Ye, Z. R. et al. Orbital selective correlations between nesting/scattering/Lifshitz transition and the superconductivity in AFe_{1-x}Co_xAs (A=Li, Na). Preprint at <http://arxiv.org/abs/1303.0682> (2013).
 - ¹⁹ Xiang, Y. Y., Wang, F., Wang, D., Wang Q. H. & Lee D. H. High-temperature superconductivity at the FeSe/SrTiO₃ interface. *Phys. Rev. B* **86** 134508 (2012).
 - ²⁰ Altieri, S., Tjengb, L.H. & Sawatzky G.A. Ultrathin oxide films on metals: new physics and new chemistry? *Thin Solid Films* **400**, 9-15 (2001).
 - ²¹ Berciu, M., Elfimov, I. & Sawatzky G.A. Electronic polarons and bipolarons in iron-based superconductors: The role of anions. *Phys. Rev. B* **79**, 214507 (2009).
 - ²² Haeni, J. H., Theis, C. D. & Schlom, D. G. RHEED intensity oscillations for the stoichiometric growth of SrTiO₃ thin films by reactive molecular beam epitaxy. *Journal of Electroceramics* **4**, 385-391 (2000).